Adsorption and Desorption of Bis-(3-sulfopropyl) Disulfide during Cu Electrodeposition and Stripping at Au Electrodes

ARTICLE *in* LANGMUIR · SEPTEMBER 2012

Impact Factor: 4.46 · DOI: 10.1021/la3025183 · Source: PubMed

6 AUTHORS, INCLUDING:

Wei-Ping Dow
National Chung Hsing University
73 PUBLICATIONS **1,415** CITATIONS

SEE PROFILE

Shuehlin Yau
National Central University
93 PUBLICATIONS **1,898** CITATIONS

SEE PROFILE

Langmuir

Article

pubs.acs.org/Langmuir

Adsorption and Desorption of Bis-(3-sulfopropyl) Disulfide during Cu Electrodeposition and Stripping at Au Electrodes

Yong-Da Chiu,[†] Wei-Ping Dow,*[,†] Klaus Krug,[‡] Yung-Fang Liu,[‡] Yuh-Lang Lee,*[,‡] and Shueh-Lin Yau*[,§]

[†]Department of Chemical Engineering, National Chung Hsing University, Taichung 40227, Taiwan

[‡]Department of Chemical Engineering, National Cheng Kung University, Tainan 70101, Taiwan

[§]Department of Chemistry, National Central University, Jhong-Li, Tao-Yuan 32001, Taiwan

Supporting Information

ABSTRACT: The adsorption and desorption of bis-(3-sulfopropyl) disulfide (SPS) on Cu and Au electrodes and its electrochemical effect on Cu deposition and dissolution were examined using cyclic voltammetry stripping (CVS), field-emission scanning electron microscopy (FESEM), and X-ray photoelectron spectroscopy (XPS). SPS dissociates into 3-mercapto-1-propanesulfonate when it is contacted with Au and Cu electrodes, producing Cu(I)- and Au(I)-thiolate species. These thiolates couple with chloride ions and promote not only the reduction of Cu^{2+} in Cu deposition but also the oxidation of Cu^0 to Cu^+ in Cu stripping. During Cu electrodeposition on the SPS-modified Au electrode, thiolates transfer from Au onto the Cu underpotential deposition (UPD) layer. The Cu UPD layer stabilizes a large part of the transferred thiolates which subsequently is buried by the Cu overpotential deposition (OPD) layer. The buried thiolates reappear on the Au electrode after the copper deposit is electrochemically stripped off. A much smaller part of thiolates transfers to the top of the Cu OPD layer. In contrast, when SPS preadsorbs on a Cu-coated Au electrode, almost all of the adsorbed SPS leaves the Cu surface during Cu electrochemical stripping and does not return to the uncovered Au surface. A reaction mechanism is proposed to explain these results.

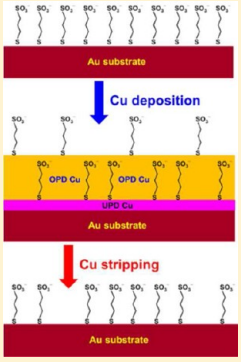

1. INTRODUCTION

Self-assembled monolayers (SAMs) of thiol molecules on coinage metal surfaces, such as Cu, Ag, and Au, are renowned for their versatile uses in many fields including sensors and metal electrodeposition.[1−3] Reports have shown that the end group of tethered thiolate admolecules can influence their adsorptive configurations, surface coverage, and stability.[3−11] At the electrodeposition front, it is found that Cu deposited onto SAM-modified Au electrodes can yield unique micrometer and nanoscale metal particles or patterns.[2,12−14]

Metal electrodeposition on SAM-modified Au electrodes was reviewed.[15,16] The chemical nature of thiol molecules adsorbed on Au electrodes can influence the mechanism of Cu deposition. However, most previous studies have focused on the underpotential deposition (UPD) of metals on SAM-modified Au substrates.[17−26] It is conceivable that SAMs greatly affect the surface-sensitive process of UPD, as exemplified for Cu and Ag heteroepitaxy on Au surfaces.[17−26] It seems that Cu and Ag atoms are deposited preferentially under the SAM to form sandwiched SAM/UPD layer/Au configurations.[17,18,20−22,25,26] In comparison, from the perspective of practical uses of electroplating, overpotential deposition (OPD) on SAM-modified Au substrates is more important but has received less attention thus far. Cavalleri et al.[19] reported that a thiol-SAM can transfer from the Au substrate onto the Cu UPD layer at high temperature but is buried by a bulk Cu deposit at room temperature.[27,28] Hagenström et al. reported that the UPD layer of Ag is deposited under the thiol-SAM, whereas the bulk Ag deposit covers the thiol adlayer.[23] Petri et al. showed that the Cu UPD layer creeps underneath the thiol-SAM, and Cu OPD is inhibited by the thiol-SAM.[24] Moffat et al. reported for homoepitaxial Cu growth that submonolayer quantities of SPS remain segregated on the growth surface even after extensive Cu deposition.[29] Molecules with a $-SO_3H$ functionality are needed for the acceleration of Cu electrodeposition because $-CH_3$-, −COOH-, and −OH-terminated thiols have been proven to be ineffective for acceleration on Cu electrodeposition.[29,30]

Recently, the Cu electrodeposition mechanism that results in bottom-up filling of vias and trenches for the integrated circuit (IC) and printed circuit fabrications has been extensively studied.[30−35] A few disulfide or thiol molecules that are preadsorbed onto a Cu or Au seed layer were enough to induce bottom-up Cu filling of vias and trenches in electroplating baths containing a suppressor species only.[30,33−35] In other words, the required amount of the thiol molecules for the vias filling process is small. Interestingly, preadsorbed thiol molecules can achieve the bottom-up Cu filling of microvias, which implies that these organic modifiers segregate on top of the Cu deposit. However, there is a lack of direct evidence that the preadsorbed thiol molecules indeed transfer from the Au seed layer onto the Cu deposit.[30,33−35]

In the present study, the thiol transfer process during the Cu deposition and stripping at a Au electrode was investigated in

Received: June 21, 2012
Revised: September 9, 2012
Published: September 15, 2012

dx.doi.org/10.1021/la3025183 | Langmuir 2012, 28, 14476−14487

detail using cyclic voltammetry (CV), scanning electron microscopy (SEM), and X-ray photoelectron spectroscopy (XPS). These results shed light on the thiol transfer behavior from the Au surface to the top of the growing Cu deposit and vice versa. Two schemes are proposed to explain the transfer mechanisms.

2. EXPERIMENTAL SECTION

2.1. Cyclic Voltammetry Stripping (CVS). Electrochemical measurements of Cu deposition and stripping at the Au electrodes were performed in a glass vessel containing 100 mL of electrolyte solution. A PGSTAT30 potentiostat (Auto-Lab) with a three-electrode cell was used at 25 °C. Au disk electrodes and Cu/Au composite electrodes (Cu film thickness ~30 nm) with a surface diameter of 3 mm were employed as working electrodes (WE). The mechanical pretreatment procedure included manually polishing the Au electrode to a mirror-finish with an alumina slurry (particle sizes of 0.5 and 0.3 μm) and a polishing cloth. Finally, the Au electrode was rinsed with deionized (DI) water and cleaned ultrasonically in DI water for 5 min to remove residual alumina particles that might be trapped on the surface. After the mechanical pretreatment, the electrode surface was examined using an optical microscope (OM, Olympus BX51) to ensure no defects. The electrochemical pretreatment was performed by successive scans between the Au redox potentials (from −0.7 to 0.9 V vs SMSE) in a 0.54 M H_2SO_4 aqueous solution at a scan rate of 50 mV s^{-1}. Usually, a stable Au redox pattern, which is the same as in previous works,[36,37] was obtained after 6 cycles, demonstrating that a clean polycrystalline Au surface had been obtained. The Au electrode was then rinsed with DI water and ultrasonicated in DI water for 5 min. The composite electrodes were prepared in a plating bath containing 0.88 M $CuSO_4$ (Riedel-de Haën, ACS-certified), 0.54 M H_2SO_4 (Merck, 96%), 200 ppm polyethylene glycol (PEG, M_w8000, Fluka), and 70 ppm Cl^- (NaCl, Fisher, ACS-certified). The counter electrode (CE) was a copper bar (99.99%). The reference electrode (RE) was a saturated mercurous sulfate electrode (SMSE). All potentials are referenced to SMSE.

The WE was immersed in an electrolyte that contained 0.88 M $CuSO_4$, 0.54 M H_2SO_4, and 5−100 ppm bis-(3-sulfopropyl) disulfide (SPS, Raschig GmbH, Germany) for 5 min. Then, the WE was transferred to another solution composed of 0.88 M $CuSO_4$, 0.54 M H_2SO_4, 200 ppm PEG (MW8000, Fluka), and 70 ppm Cl^- for the CVS analysis. For SPS-modified Au electrodes, the potential was scanned from the open circuit potential (OCP) (zero current at electrode; 0.0 V) to −0.7 V and back to 0.6 V (or 0.1 V). For SPS-modified Cu/Au electrodes, the potential was scanned from the OCP (−0.37 V) to 0.1 V and back to −0.7 V. The scan rate varied from 0.5 to 50 mV s^{-1}.

2.2. Field-Emission Scanning Electron Microscopy (FESEM). The surface morphologies of the Cu films during stripping were examined at specific potentials of the CVS experiments and imaged using a field-emission scanning electron microscope (FESEM, JEOL, JSM-7401F). When the potential of the SPS-modified Cu/Au electrode was scanned from the OCP to −0.3 V in the CVS experiment, the sample was taken out of the CVS cell and put in a bag charged with nitrogen gas, in order to avoid possible surface oxidation of these samples before these samples were transferred into the vacuum chamber of FESEM. FESEM reveals valuable information about the surface status and residual species at the interface.

2.3. X-ray Photoelectron Spectroscopy (XPS). The electrode sample was first dried in a nitrogen stream and then transferred into an ultrahigh vacuum (UHV) chamber maintained at a pressure of 2.2 × 10^{-7} Pa. The XPS spectrometer was a PHI 5000 VersaProbe using monochromatic Al Kα radiation. XPS spectra were recorded at a takeoff angle (TOA) of 45° with 58.7 eV of pass energy, 22.1 W of electron-beam power, a 0.1 mm beam size, and a resolution of 0.2 eV. Additional spectra were acquired at TOAs of 15°, 45°, and 90° to study the spatial distribution of sulfur-containing elements on the substrate surface. The bulk Au 4f core level (84.00 eV) and the Cu 2p core level (932.6 eV) were used as references to determine the binding energies in the XPS spectra. XPS PEAK (version 4.1) was used to fit Gaussian−Lorentzian functions on a linear background to the XPS spectra.

3. RESULTS AND DISCUSSION

3.1. Cyclic Voltammetry Stripping. Figure 1 shows the CVS results of an SPS-modified Au electrode in 0.54 M H_2SO_4

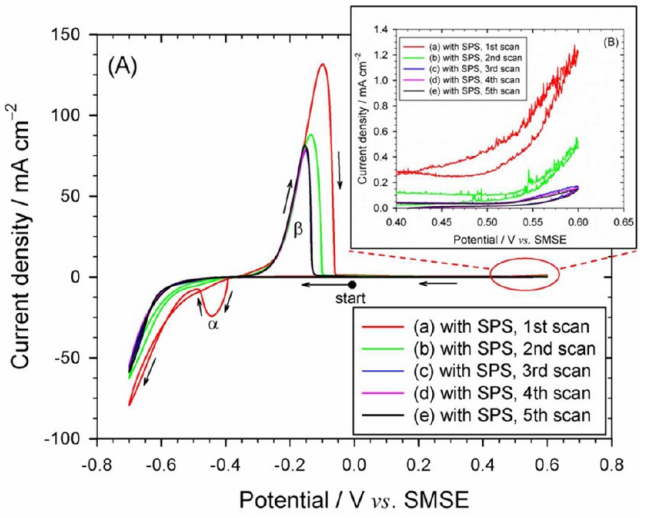

Figure 1. Cu CVS on Au electrode modified by soaking in 5 mM SPS for 5 min. The electrolyte contained 0.88 M $CuSO_4$, 0.54 M H_2SO_4, 200 ppm PEG, and 70 ppm Cl^- at 25 °C. The potential scan sequence was OCP (0.0 V) → −0.7 V → to 0.6 V → OCP with a scan rate of 5 mV s^{-1}.

containing 0.88 M $CuSO_4$, 200 ppm PEG, and 70 ppm Cl^-. The potential was initially held at the OCP (0.0 V) and then cycled 5 times between −0.7 and 0.6 V (dE/dt = 5.0 mV/s). The reductive peak, α, at −0.45 V appears only in the first cycle. The α peak results from the formation of Cu nanoparticles (CuNPs) on the SPS-modified Au electrode.[38] Cu(I)-thiolate-Cl complexes, coming from SPS + 2Cu + 2Cl^- → 2Cu(I)-thiolate-Cl^-, adsorbed on specific sites are confirmed by STM images and responsible for the acceleration of copper nucleation and deposition.[39,40] The detailed mechanism of SPS dissociation on Cu and Au electrodes to form Cu(I)-thiolate-Cl on Cu and Au electrodes are reviewed in the previous work.[39] The oxidative peak, β (−0.1 V), is attributed to Cu film stripping. Since the potential was scanned to 0.6 V, oxidative desorption of SPS admolecules occurred,[41−43] which results in a successive decrease in the anodic current density with the number of potential cycles (Figure 1B). During the anodic potential sweep, parts of the adsorbed thiolates (i.e., SPS dissociation) were electrochemically oxidized and the accelerating effect on Cu deposition, induced by thiolates and chloride ions, gradually decreases. This is indicated by the disappearance of the α peak and the decrease of the β peak after the first potential cycle. With less thiolates, the inhibition effect of PEG + Cl^- on the Cu-deposition process becomes more dominant.[44−48]

Figure 2 shows CVS profiles obtained under the same experimental conditions with the exception that the scan rate was varied from 0.5 to 50 mV/s, and the positive return potential was set to 0.1 V. Independent of the scan rate, the α peak is present in five consecutive cycles and the peak area decreases slowly with each cycle (Figures 2B, D, and F). These

dx.doi.org/10.1021/la3025183 | Langmuir 2012, 28, 14476−14487

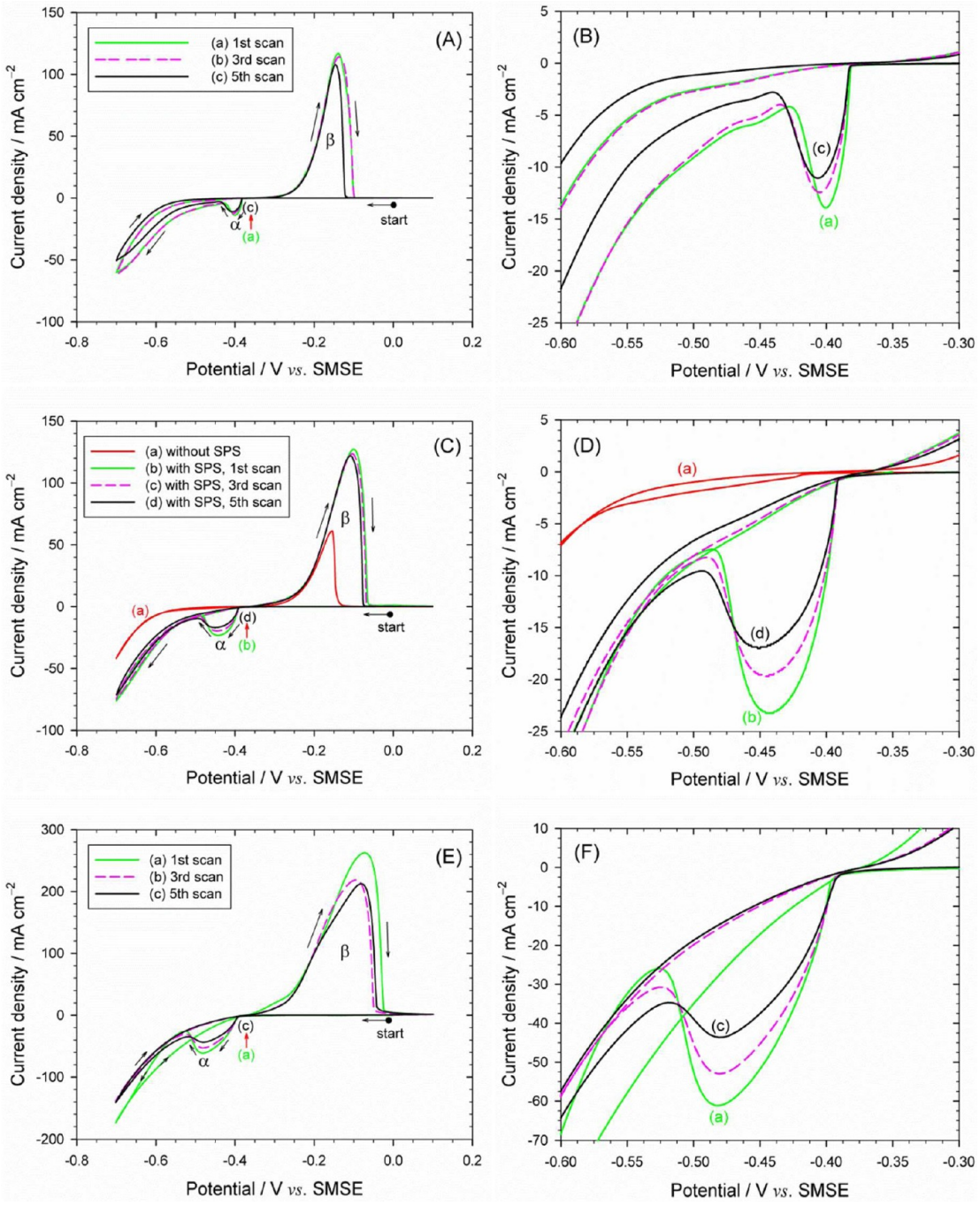

Figure 2. Cu CVS on Au electrode at different scan rates. The Au electrode was modified by a SPS adlayer by dipping in 5 ppm SPS for 5 min. The Cu CVS was carried out in an electrolyte solution containing 0.88 M $CuSO_4$, 0.54 M H_2SO_4, 200 ppm PEG, and 70 ppm Cl^- at 25 °C. The potential scan proceeded in the sequence OCP (0.0 V) → −0.7 V → 0.1 V → OCP. The scan rates are (A and B) 0.5 mV s^{-1}, (C and D) 5.0 mV s^{-1}, and (E and F) 50.0 mV s^{-1}.

results indicate that the SPS adlayer still exists after several Cu-deposition and Cu-stripping cycles. This is in strong contrast to the result shown in Figure 1, where the α peak was seen only in the first negative sweep. The larger stripping peak β and the α-peak appearance in SPS-containing systems (compare the curves b−d with curve a in Figure 2C) reflect that the interaction of SPS and Cl^- not only promotes Cu nucleation but also facilitates copper deposition.[49−52]

Figure 3 summarizes the integrated charge of the α peak as inferred from the CVS profiles (Figure 2). It is found that the intensity of the α peak decreases by 7.1% after five potential cycles at the scan rate of 0.5 mV/s, whereas a 50.6% decrease is observed at the scan rate of 50 mV/s. These findings imply that at low scan rates nearly all of the originally adsorbed SPS molecules turn into thiolates[49,51−54] (also see the following XPS analyses), and these thiolates transfer slowly onto the Cu UPD layer because thiolates interact more strongly with the Cu UPD layer than with the Au electrode.[55−57] A few thiolates can successively transfer onto the Cu OPD layer within the reductive potential scan, while most thiolates become buried below the Cu OPD layer. When the potential is changed to the regime of Cu dissolution, these thiolates adsorbed on the Cu

dx.doi.org/10.1021/la3025183 | *Langmuir* 2012, 28, 14476−14487

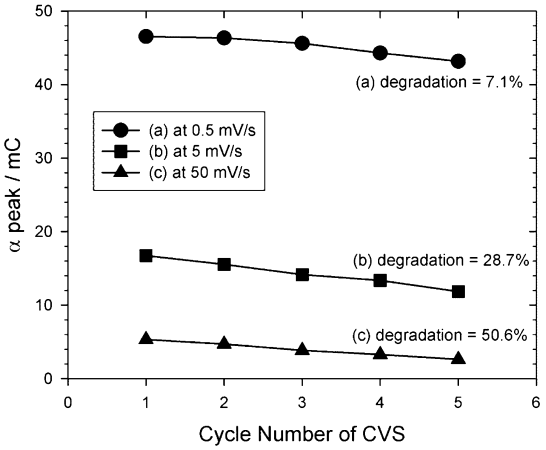

Figure 3. Evaluation of α peak in CVS with cycle number at different scan rates. The charge associated with the α peak was obtained from Figure 2. The scan rates are (a) 0.5 mV s^{-1}, (b) 5.0 mV s^{-1}, and (c) 50.0 mV s^{-1}.

OPD layer do not easily remain on the Cu surface. However, after the completion of the Cu-stripping process, almost all of the buried thiolates that are pinned by the Cu UPD layer readsorb on the bare Au surface, leading to the small charge decrease of the α peak in subsequent potential cycles. In comparison, faster scan rates provide shorter time periods for thiolates to relocate so that they leave the interface with the formation of a Cu UPD layer and the stripping of a Cu OPD layer, rather than return to the Au electrode after five cycles in CVS.

These results are in agreement with the electrochemical reductive desorption of thiolates [i.e., R−S-Au + H^+ + e^- → R−SH + Au, R−SH = 3-mercapto-1-propanesulfonate (MPS)][26,40,53,58] and with the kinetics-controlled readsorption.[22] Therefore, the transfer rate of the adsorbed thiolates from the Au electrode onto the Cu UPD layer is slow. In addition, Cu adatoms can creep underneath the SAM to form a more favorable SAM/Cu/Au sandwich structure.[55−57] The SAM on top of the Cu UPD layer is more resistant to reductive desorption than that on a Cu-free Au electrode.[55−57] The sandwich-structure formation process is also kinetics-controlled. Consequently, higher scan rates result in broader and smaller α peaks, which is consistent with the kinetics-controlled processes of the thiolates readsorption and the Cu UPD layer formation.

3.2. Cu CVS on Au Electrode from Stripping to Deposition. To explore the effect of the Cu UPD layer on the stability of the SPS adlayer, we conducted voltammetric experiments with the Cu/Au composite electrodes. The potential scan sequence was OCP (−0.37 V) → 0.1 V (for Cu stripping) → −0.7 V (for Cu deposition). Figure 4A shows CVS profiles of an unmodified Cu/Au sample in 0.54 M H_2SO_4 containing 0.88 M $CuSO_4$, 200 ppm PEG, and 70 ppm Cl^-. Following the first cycle, the CVS curves are stable in each potential cycle and the intensity of the β peak is constant in the employed potential window. By contrast, CVS profiles recorded for SPS-modified Cu/Au electrodes reveal the presence of the α peak whose intensity decreases with each potential cycle (Figure 4, panels B−E). Obviously, the α peak in Figure 4 is much smaller than those in Figures 1 and 2. The corresponding charge values of these α peaks are calculated and shown in Figure S1 of the Supporting Information. The Cu-stripping peak appears as a single peak β in the first cycle of bare Cu/Au electrodes (curve a in Figure 4A) but splits into two peaks (δ and γ) for the SPS-modified Cu/Au electrodes (curves a in Figure 4, panels B−E). The peak potentials of δ (−0.32 V) and γ (−0.25 V) are more negative than that of the β peak (−0.22 V). This negative shift in potential is thought to arise from a promoting effect of SPS admolecules on the dissolution of the Cu deposit. Also, the appearance of the α peak suggests that the SPS molecules originally adsorbed on the Cu film transfer to the Au substrate after the Cu deposit dissolves. Higher SPS concentrations in the predipping bath lead to more pronounced α peaks, as shown in Figure S1 of the Supporting Information, indicating a higher SPS coverage on the Cu film. The potential ranges of Cu UPD in Figures 2 and 4 are shown in Figures S2 and S3 of the Supporting Information, respectively.

On the basis of the data shown in Figure 2C (i.e., SPS/Au) and Figure 4, panels B−E (i.e., SPS/Cu/Au), it is clear that the β peak decreases with the potential cycles. This phenomenon depends not only on the SPS concentration but also on the chemical nature of the electrode. Figure 5A shows the integrated charge of the β peak as a function of the potential cycle for various electrodes and SPS concentrations in the predipping bath. It appears that low SPS concentrations yield more pronounced decreases (Figure 5B). However, this trend does not hold for the SPS-modified Au electrodes (red solid circles in Figure 5A), as the β peak reduces by only 14.4% after 5 cycles (Figure 5B, case a). It is likely that the SPS adlayer remains on the electrode after five potential cycles between −0.7 and 0.1 V, even if the dosing concentration of SPS is as low as 5 ppm. The difference between the SPS-modified Au electrodes and the SPS-modified Cu/Au electrodes is that in the former case the formation of the Cu UPD layer occurs in the first cycle with an SPS adlayer transfer from the Au surface to the Cu monolayer, while in the latter case Cu OPD layer stripping occurs with oxidative desorption of the SPS adlayer. Hence, the α peak is pronounced after five cycles in the CVS of SPS-modified Au (Figure 2), but disappears after the first cycle in the CVS of SPS-modified Cu/Au electrodes (Figure 4).

Figure 6 summarizes the first CVS profiles recorded for SPS-modified Cu/Au electrodes with the potential scanned positively from the OCP (−0.37 V) to 0.1 V, then reversed to −0.7 V, and finally returned to the OCP (−0.37 V). The electrodes were modified in predipping baths containing 0−100 ppm SPS. It is important to note that the α peak does not appear in the absence of an SPS adlayer.[38] The Cu-stripping peaks of SPS-modified electrodes are all shifted negatively and split into two peaks, δ and γ. The negative potential shift suggests that the SPS adlayer promotes Cu oxidation. This phenomenon was observed only in the presence of chloride ions. It was reported that a Cu electrode can be oxidized in two steps [i.e., Cu → Cu(I) → Cu(II)] in the presence of chloride ions.[59,60] Láng et al.[61] and Doblhofer et al.[62] employed an EQCM to confirm that a two-step copper dissolution [i.e., Cu → Cu(I) → Cu(II)] occurs if chloride ions are present in the electrolyte during copper stripping. A transition oxidation state of copper is present in the form of $CuCl_{(ad)}$. The generated amount of $CuCl_{(ad)}$ during electrochemical copper dissolution depends on the chloride ion concentration. The higher the chloride ion concentration, the larger the amount of CuCl that will be obtained. In addition, Okubo et al.[63] employed a RRDE to confirm that the Cu(I) species are easily formed during copper dissolution in the presence of SPS and the chloride ions. High SPS concentration results in more Cu(I) species during

dx.doi.org/10.1021/la3025183 | Langmuir 2012, 28, 14476−14487

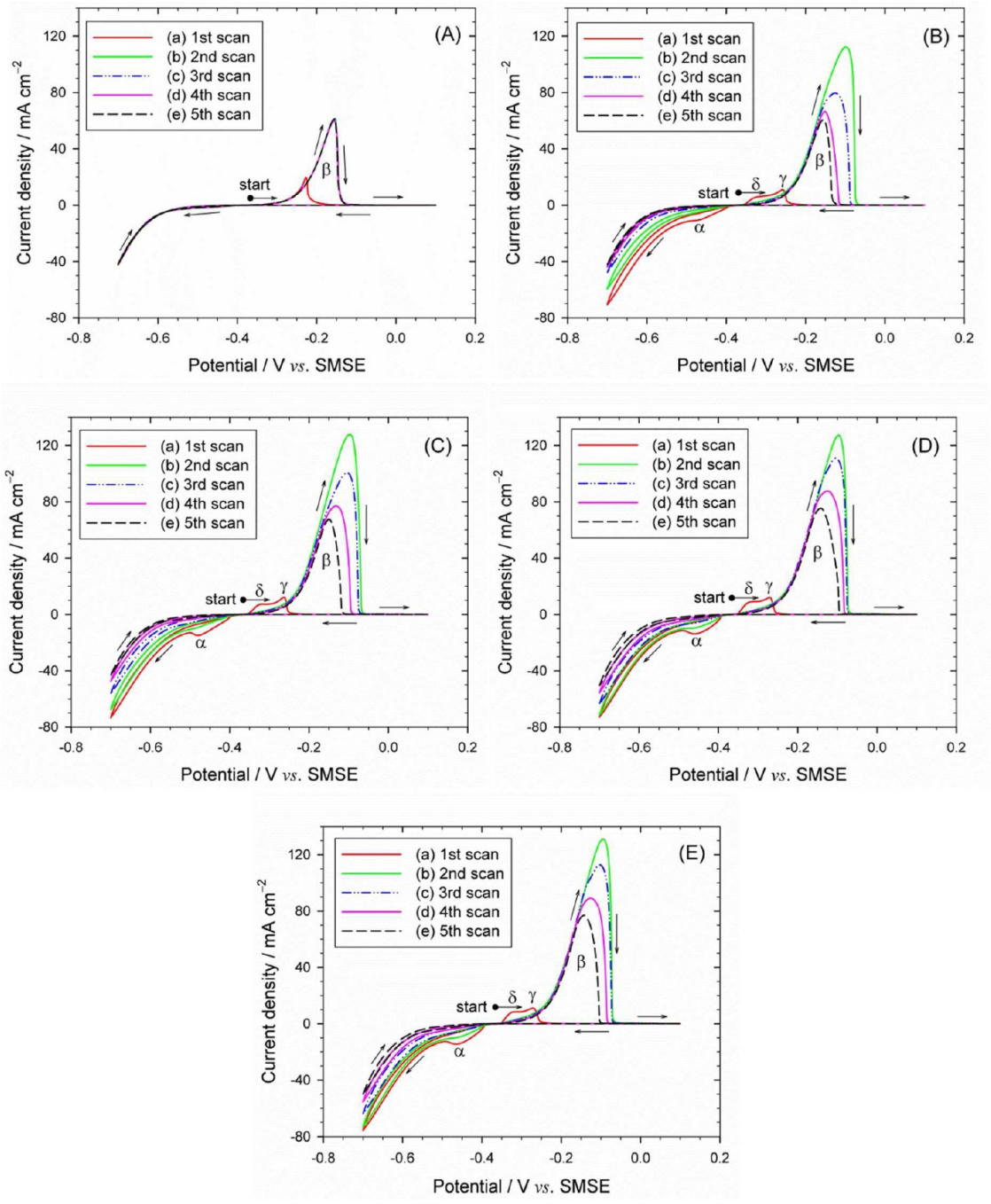

Figure 4. Cu CVS on Cu-coated Au electrode. The electrolyte used was 0.88 M $CuSO_4$, 0.54 M H_2SO_4, 200 ppm PEG, and 70 ppm Cl^- at 25 °C. The SPS concentration in the preadsorption solution was (A) 0, (B) 5, (C) 45, (D) 80, and (E) 100 ppm. The potential scan sequence was OCP (−0.37 V) → 0.1 V → −0.7 V → OCP with a scan rate of 5 mV s^{-1}.

copper dissolution in the presence of a chloride ion. They concluded that a transition state of CuCl is always formed regardless of the copper deposition and dissolution, as long as both SPS and chloride ions are present in the electrolyte. Formation of the Cu(I) species is strongly related to a chemical interaction between SPS and the chloride ion. These results strongly support the assignments of the δ and γ peaks herein. However, the single oxidation peak in the CVS of the SPS-free system (curve a in Figure 6) does not indicate the two-step process, even though chloride ions are present. This behavior is attributed to the presence of PEG, which can interact with the chloride ions to form a PEG−Cl complex,[44−48] such that $CuCl_{(ad)}$ is not easily formed in the presence of PEG.[48]

Many reports have shown that the synergism of SPS and Cl^- facilitates electron transfer in the process of Cu^{2+} reduction.[38,49−52] This view is consistent with the appearance of the α peak in the presence of SPS and Cl^- (Figure 6).[38] On the other hand, the synergism of SPS and Cl^- seems effective also for facilitating electron transfer in Cu stripping as follows

$$RSSR_{(aq)} + 2Cu_{(s)} \rightarrow 2RSCu(I)_{(ad)}\cdots \quad (1)$$

(during chemical adsorption)

dx.doi.org/10.1021/la3025183 | *Langmuir* 2012, 28, 14476−14487

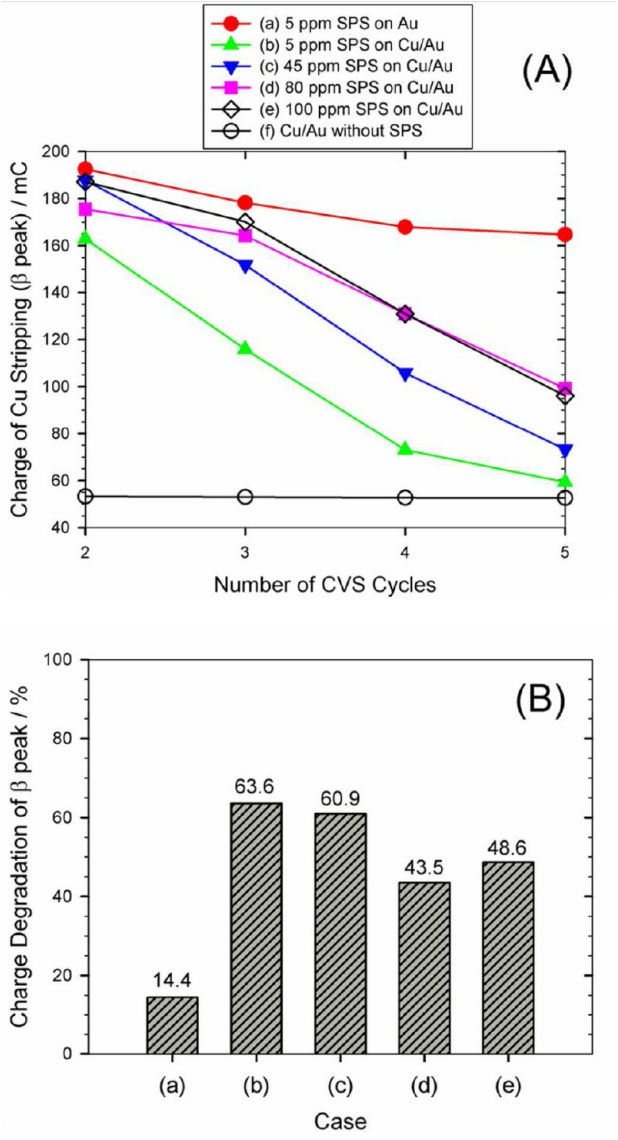

Figure 5. Evaluation of β peak in CVS with cycle number on different working electrodes. The charge of the β peak was obtained from Figure 4. The charge degradation of the β peak is defined as [(stripping charge of the second cycle) − (stripping charge of the fifth cycle)/(stripping charge of the second cycle)] × 100%. The cases shown in Figure B are the same as those shown in Figure A.

$$RSCu(I)_{(ad)} + H^{+}_{(aq)} \rightarrow Cu^{2+}_{(aq)} + RSH_{(aq)} + e^{-}\ldots \quad (2)$$

(during Cu stripping)

$$Cu_{(s)} \rightarrow Cu^{+}_{(ad)} + e^{-}\ldots \quad (3)$$

(during Cu stripping)

$$RSH_{(aq)} + Cu^{+}_{(ad)} \rightarrow RSCu(I)_{(ad)} + H^{+}_{(aq)}\ldots \quad (4)$$

(during Cu stripping)

$$RSCu(I)_{(ad)} + HCl_{(aq)} \rightarrow RSH_{(aq)} + CuCl_{(ad)}\ldots \quad (5)$$

(during Cu stripping)

$$CuCl_{(ad)} \rightarrow Cu^{2+}_{(aq)} + Cl^{-}_{(aq)} + e^{-}\ldots \quad (6)$$

(during Cu stripping)Reaction 1 represents the dissociative adsorption of SPS on the Cu/Au electrode, leading to Cu(I)-thiolates adsorbed on the copper surface during the preadsorption step.[39,49,51,52,54] Reaction 2 represents the electrochemical oxidation of the adsorbed Cu(I)-thiolates to Cu(II) and MPS formation due to Cu(I) oxidation.[39] Reaction 3 is the electrochemical oxidation of Cu to Cu(I). Desorbed thiols (i.e., MPS) return to the copper surface during copper stripping and react with the adsorbed Cu(I) coming from reaction 3 to form Cu(I)-thiolates (Reaction 4). Reaction 5 represents the formation of $CuCl_{(ad)}$ from the reaction of Cu(I)-thiolates with chloride ions.[39,50,52,63,64] Reaction 6 is the electrochemical oxidation of $CuCl_{(ad)}$ to Cu(II).[39,63,64] Scanning tunneling microscopy (STM) studies have shown that ordered and dense adsorption structures of MPS due to SPS dissociation are easily observed on Au(111) at the anodic (i.e., oxidative) potential because of the negative charge of the thiolate and sulfonic acid groups.[52,58] Accordingly, reactions 3 and 4 are accelerated at an anodic potential. The interactions between MPS and the chloride ions, which are important for the acceleration of the Cu electrochemical oxidation to form $CuCl_{(ad)}$, are described by the reactions 4 and 5.[39,50,52,63,64]

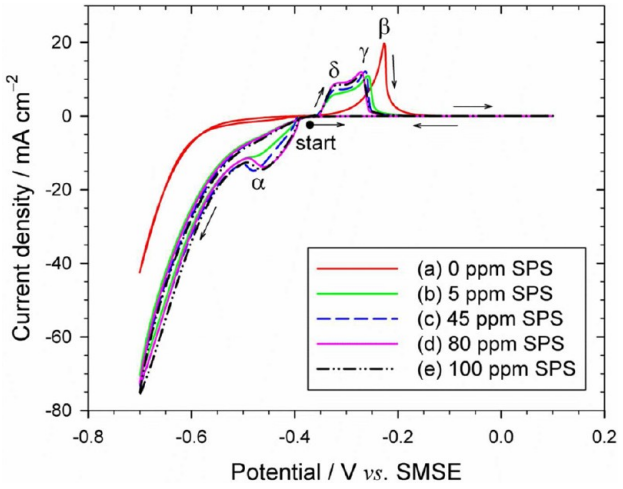

Figure 6. Cu CVS on Cu/Au electrode. The electrolyte contained 0.88 M $CuSO_4$, 0.54 M H_2SO_4, 200 ppm PEG, and 70 ppm Cl^- at 25 °C. The SPS concentration in the preadsorption solution was (a) 0, (b) 5, (c) 45, (d) 80, and (e) 100 ppm. The potential scan sequence was OCP (−0.37 V) → 0.1 V → −0.7 V → OCP with a scan rate of 5 mV s^{-1}.

To substantiate the two-step oxidation mechanism of the SPS-modified Cu film, the Cu-stripping peaks were deconvoluted into two peaks, δ and γ. Figure S4 of the Supporting Information shows the original data and the deconvoluted peaks, respectively. The corresponding integrated charges are listed in Table 1. It is found that δ and γ contribute equally to the Cu-stripping peak, independent of the SPS concentration. These results indicate that SPS admolecules facilitate Cu(I) formation, which is in agreement with these previous works.[39,63] Chloride ions can promote the electron release of Cu to form Cu(I) through an inner-sphere electron transfer process.[65,66] However, when both SPS and the chloride ions are simultaneously present, crystalline $CuCl_{(s)}$ rather than a CuCl precursor or cluster is formed.[48,64] Crystalline $CuCl_{(s)}$ is known to block Cu corrosion.[67−69] The formation and oxidation of the mediate phases [i.e., thiolate-Cu(I) and CuCl], as proposed by the reactions 1, 2, and 4−6, are responsible for the formation of the δ and γ peaks. Table 1 shows that the charge of the δ peak is similar to that of the γ peak, and the total charge is almost the same in each Cu-stripping experiment.

dx.doi.org/10.1021/la3025183 | Langmuir 2012, 28, 14476−14487

Table 1. Analysis of Cu-Stripping Peaks in the CVS Experiments

SPS concentration (ppm)	peak area[a] (%)		ratio[b]
–	δ	γ	$(\gamma+\delta)/\beta$
0	0	0	–
5	55.7	51.7	0.97
45	49.9	51.4	0.98
80	48.6	53.3	1.01
100	47.5	52.3	1.03

[a]Peak areas of δ and γ (fits in Figure S4 of the Supporting Information) are normalized to the total area of the double peak (numerical integration). [b]The ratio of peak areas, $(\delta + \gamma)/\beta$, obtained from Figure 6.

3.3. FESEM Micrographs of Cu Deposit on Gold Electrode. Figure 7 shows high resolution FESEM images of Cu/Au electrodes prepared under different conditions. The surface morphology of the Cu deposit without the SPS adlayer is shown in Figure 7a. Cu islands (i.e., mountains) with a size of ca. 50 nm are clearly seen. Figure 7b was obtained after the potential was shifted to −0.3 V (i.e., to the valley potential between the δ and γ peaks). The corresponding current density of copper dissolution at −0.3 V is about 1.5 mA cm^{-2} (see Figure S5 of the Supporting Information). The corresponding Cu deposit has a spongelike appearance with a lot of nanopores. The Cu film dissolution is uniform, although an overall pitted surface appears. Therefore, only the β peak is observed in the CVS pattern, which is attributed to Cu oxidation to Cu(II).

If the Cu-coated Au electrode was modified with 5 ppm SPS for 5 min, the surface morphology in Figure 7c was obtained. Compared to Figure 7a, the Cu crystal size is significantly smaller. This is attributed to the corrosion effect of SPS, as described by reactions 1 and 2 and confirmed by electron paramagnetic resonance (EPR) measurements.[70] The surface morphology of this electrode was examined again after the potential was shifted to −0.3 V (i.e., to the valley between the δ and γ peaks) (Figure 7d). The corresponding current density of copper dissolution at −0.3 V is always higher than 7.0 mA cm^{-2} (see Figure S4 of the Supporting Information), indicating that thiolates indeed can interact with chloride to facilitate copper dissolution. The morphology after partial Cu dissolution is still similar to the original appearance in Figure 7c but very different from the partially dissolved Cu film in the SPS-free system (Figure 7b). These results indicate that SPS-covered Cu films dissolve nonuniformly. We propose that Cu dissolves faster at surface areas which are covered by the MPS−Cl complexes[26,38,49−52] to form valleys and slower at surface areas which are covered by PEG−Cl complexes[44−48] and $CuCl_{(s)}$[67−69] to form mountains.

These results also indicate that thiolates may be removed during the Cu-stripping process. Therefore, a few thiolates can survive the dissolution of the Cu film. This is consistent with the CVS curves in Figure 4. However, when the thiolates are preadsorbed on the Au electrode rather than on the Cu/Au

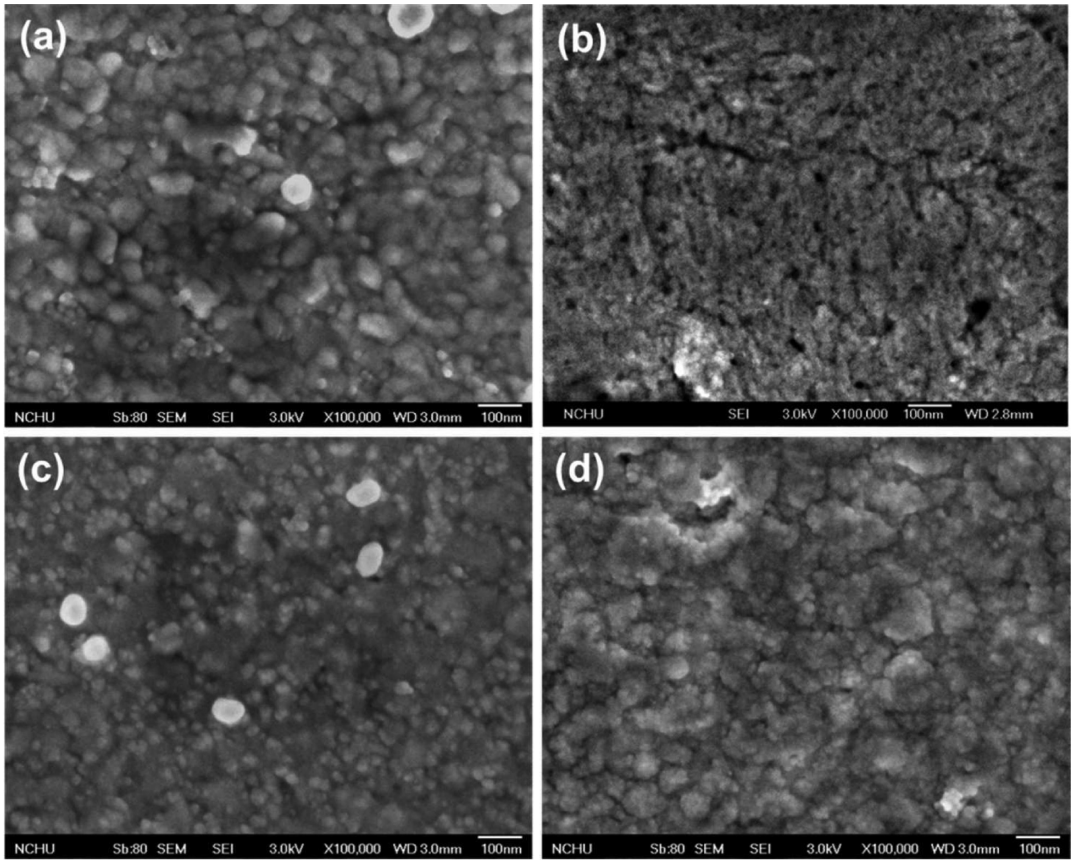

Figure 7. FESEM images of Cu deposit morpologies. (a) Bare Cu/Au composite electrodes; (b) sample (a) after electrochemical stripping by an anodic potential sweep from OCP (−0.37 V) to −0.3 V; (c) sample (a) after immersion in SPS-containing solution (5 ppm) for 5 min; and (d) sample (c) after electrochemical stripping by an anodic potential sweep from OCP (−0.37 V) to −0.3 V.

dx.doi.org/10.1021/la3025183 | *Langmuir* 2012, 28, 14476−14487

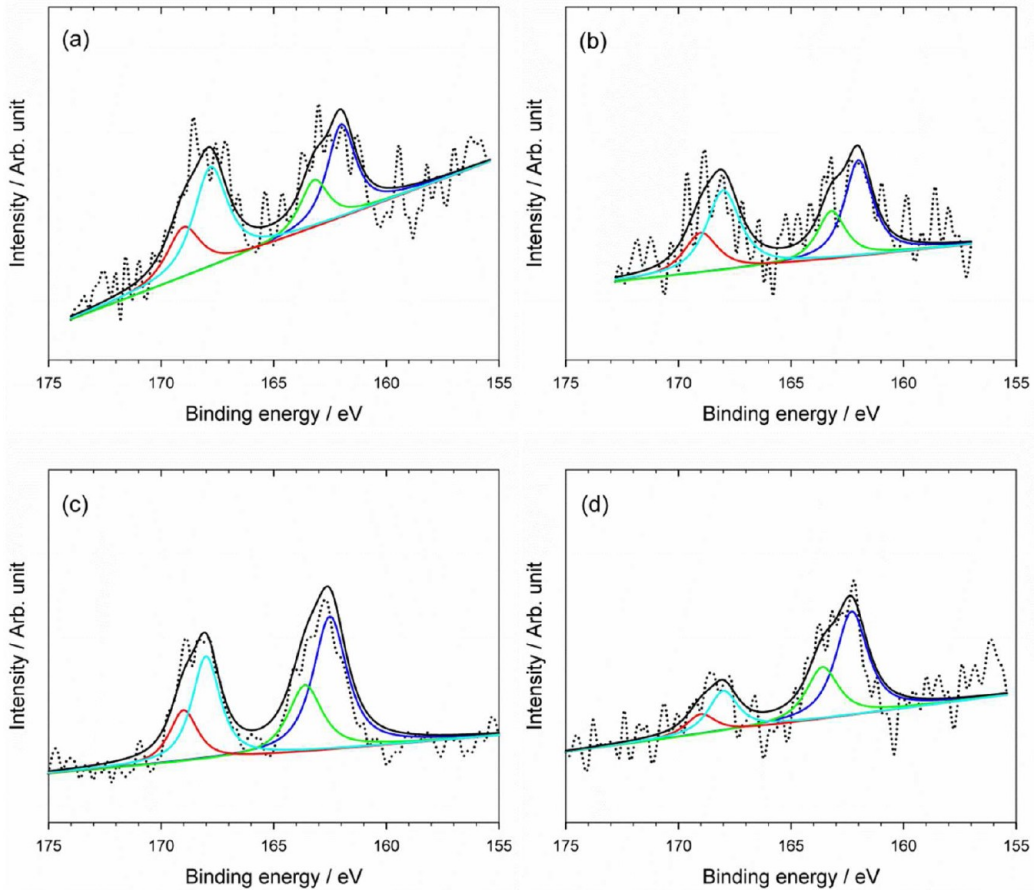

Figure 8. XPS spectra in the S(2p) region. (a) Au electrode after immersion in 5 ppm SPS solution for 5 min; (b) Au electrode after immersion in 10 ppm SPS solution for 5 min; (c) Cu/Au electrode after immersion in 100 ppm SPS solution for 5 min; and (d) Au electrode after immersion in 10 ppm SPS solution for 5 min and subsequent potential sweep from the OCP to −0.5 V (Cu OPD regime) with a scan rate of 5 mV s^{-1}.

composite electrode, most of the thiolates reappear in subsequent potential cycles. The difference in both cases is the concentration of SPS on top of the Cu UPD layer which is high on the SPS-modified Au electrode after Cu UPD layer growth and low on the SPS-modified Cu/Au electrode after stripping of the Cu OPD layer. This is because the Cu UPD layer formed on the SPS-modified Au electrode stabilizes the transferred thiolates against electrochemical reduction (i.e., desorption) during the cathodic scan (Cu deposition) and electrochemical oxidation during the anodic scan (Cu dissolution). Consequently, the charge degradation of the β-peak after five potential cycles is always larger for CVS experiments started from SPS/Cu OPD layer/Au electrodes (Figure 5A, curves b−e) than for CVS experiments started from SPS/Au electrodes (Figure 5A, curve a).

3.4. XPS Analysis. To clarify the adsorption and transfer mechanism of SPS on Cu and Au surfaces, we employed the XPS technique to examine the interfacial composition of the samples at different potentials in the CVS analysis. The XPS results obtained for S(2p) signals are summarized in Table S1 of the Supporting Information.[71−86]

3.4.1. SPS Adsorption on Au Electrodes. When the Au electrode was immersed for 5 min in the solutions containing 5 and 10 ppm SPS, S(2p) signals appeared at 162 eV [$S(2p_{3/2})$] and 163.2 eV [$S(2p_{1/2})$], as shown by the dark-blue and green lines in Figure 8, panels a and b, respectively. In addition, the SO_3^- functionality resulted in two peaks at 168 eV [$S(2p_{3/2})$] and 169 eV [$S(2p_{1/2})$], as shown by the light-blue and red lines in Figure 8, panels a and b, respectively. These results indicate that the S−S bond of SPS cleaves after SPS attaches to the Au surface (i.e., one SPS molecule breaks down into two 3-mercapto-1-propanesulfonate (MPS) molecules) which is in agreement with the following reaction proposed in literature[26,53,58]

$$SPS_{(aq)} + 2Au_{(s)} \rightarrow 2MPS - Au(I)_{(ad)}... \quad (7)$$

3.4.2. SPS Adsorption on Cu/Au Electrodes. For Cu-coated Au electrodes immersed in 100 ppm SPS for 5 min, XPS results reveal a S(2p) signal at 162 eV [$S(2p_{3/2})$] and 163.6 eV [$S(2p_{1/2})$] attributed to S−Cu bonds, as shown by the dark-blue and green lines in Figure 8c. This feature is accompanied by two additional peaks at 168 eV [$S(2p_{3/2})$] and 169 eV [$S(2p_{1/2})$], as shown by the light-blue and red lines in Figure 8c. The latter peaks are attributed to bonds between SO_3^- species and aliphatic chains. These results indicate that the disulfide bond (S−S) of SPS cleaves upon molecular adsorption on the Cu deposit, presumably yielding MPS admolecules (i.e., thiolates), as described by reaction 1.[39,49,51,52,54]

3.4.3. SPS Transfer from Au to Cu OPD Layer. When the Au electrode was immersed in a solution containing 10 ppm SPS for 5 min and then transferred into the CVS cell to perform a cathodic potential scan from the OCP to −0.5 V (Figure 8d), S−Cu bonds are observed at binding energies of 162 eV for $S(2p_{3/2})$ (dark-blue line) and 163.6 for $S(2p_{1/2})$ (green line). In addition, C−SO_3^- bonds are observed at the binding energies of 168 eV for $S(2p_{3/2})$ (light-blue line) and 169 eV for $S(2p_{1/2})$

dx.doi.org/10.1021/la3025183 | *Langmuir* 2012, 28, 14476−14487

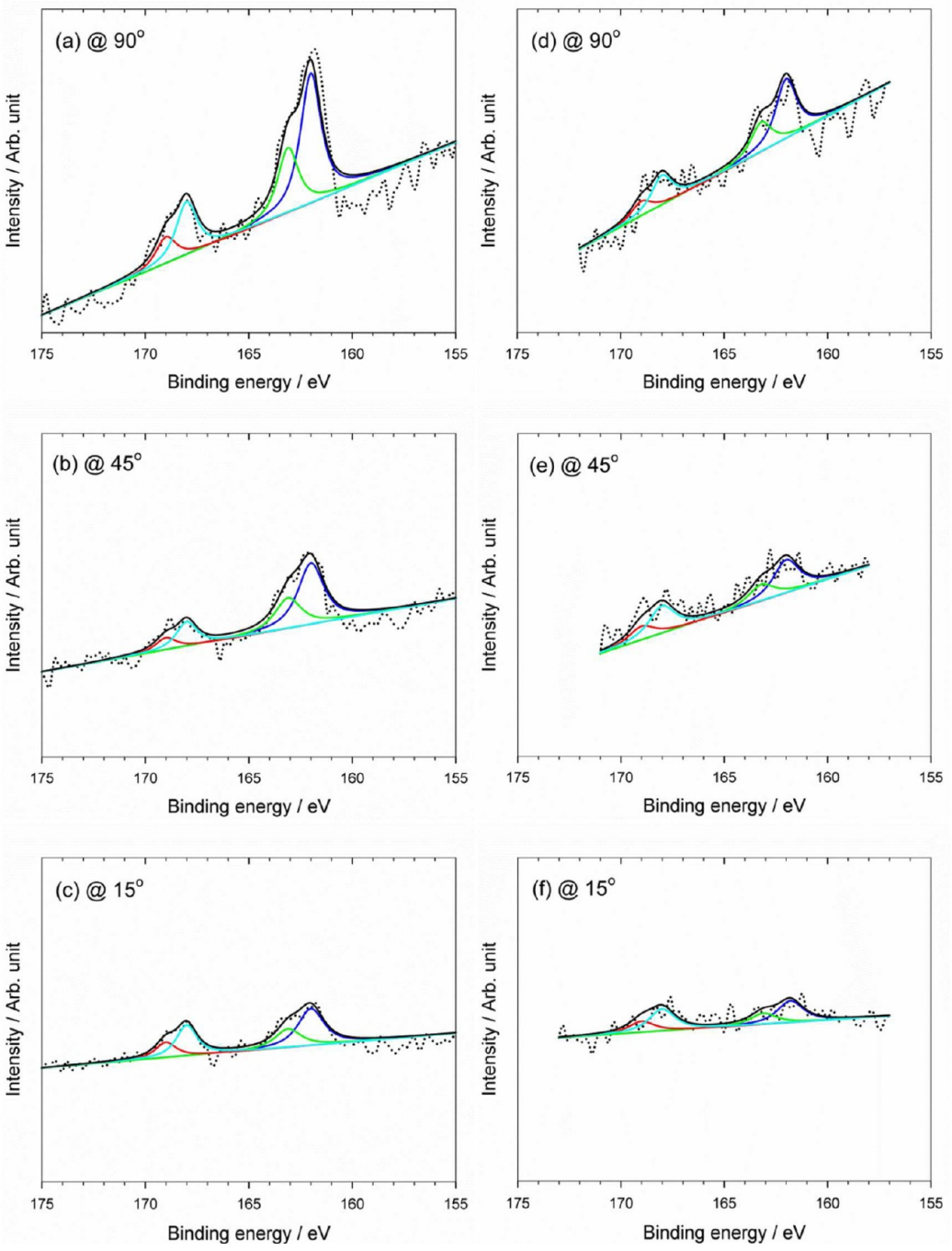

Figure 9. XPS spectra in the S 2p region at different TOAs. (a–c) Au electrode after immersion in 10 ppm SPS solution for 5 min and subsequent potential sweeps from the OCP (0.0 V) to −0.5 V and back to 0.1 V at a scan rate of 5 mV s^{-1}; (d–f) Cu/Au electrode after immersion in 100 ppm SPS solution for 5 min and a subsequent potential sweep from the OCP to 0.1 V (Cu stripping) at a scan rate of 5 mV s^{-1}.

(red line). These results indicate that the preadsorbed thiolates transfer (at least partly) from the Au surface onto the surface of the Cu OPD layer during Cu growth.

3.4.4. SPS Transfer from Cu OPD Layer to Au. In order to investigate the transfer of thiolates from the surface of the Cu OPD layer to the Au surface, XPS experiments were carried out for two samples "A" and "B" at different TOAs. Sample A is a Au electrode that was first immersed in a solution containing 10 ppm SPS for 5 min and then transferred into the CVS cell. Subsequently, a Cu OPD film was deposited by a cathodic potential sweep from the OCP to −0.5 V, and the entire Cu film was stripped by an anodic sweep to 0.1 V. Sample B is a Cu/Au composite electrode that was first immersed in the solution containing 100 ppm SPS for 5 min and then transferred into the CVS cell. The initial Cu film was directly stripped by an anodic potential sweep from the OCP to 0.1 V. Finally, the surfaces of both samples (A and B) were free of Cu atoms.

Figure 9 shows the corresponding XPS data. Only sample A exhibits strong S(2p) signal intensities for S–Au and C–SO_3^- bonds. Especially, at low TOA (15 °), the S(2p) signal intensity from both bonds is still pronounced for sample A (Figure 9c), whereas only an extremely weak S(2p) signal intensity is observed for the C–SO_3^- bond of sample B (Figure 9f). The

dx.doi.org/10.1021/la3025183 | *Langmuir* 2012, 28, 14476–14487

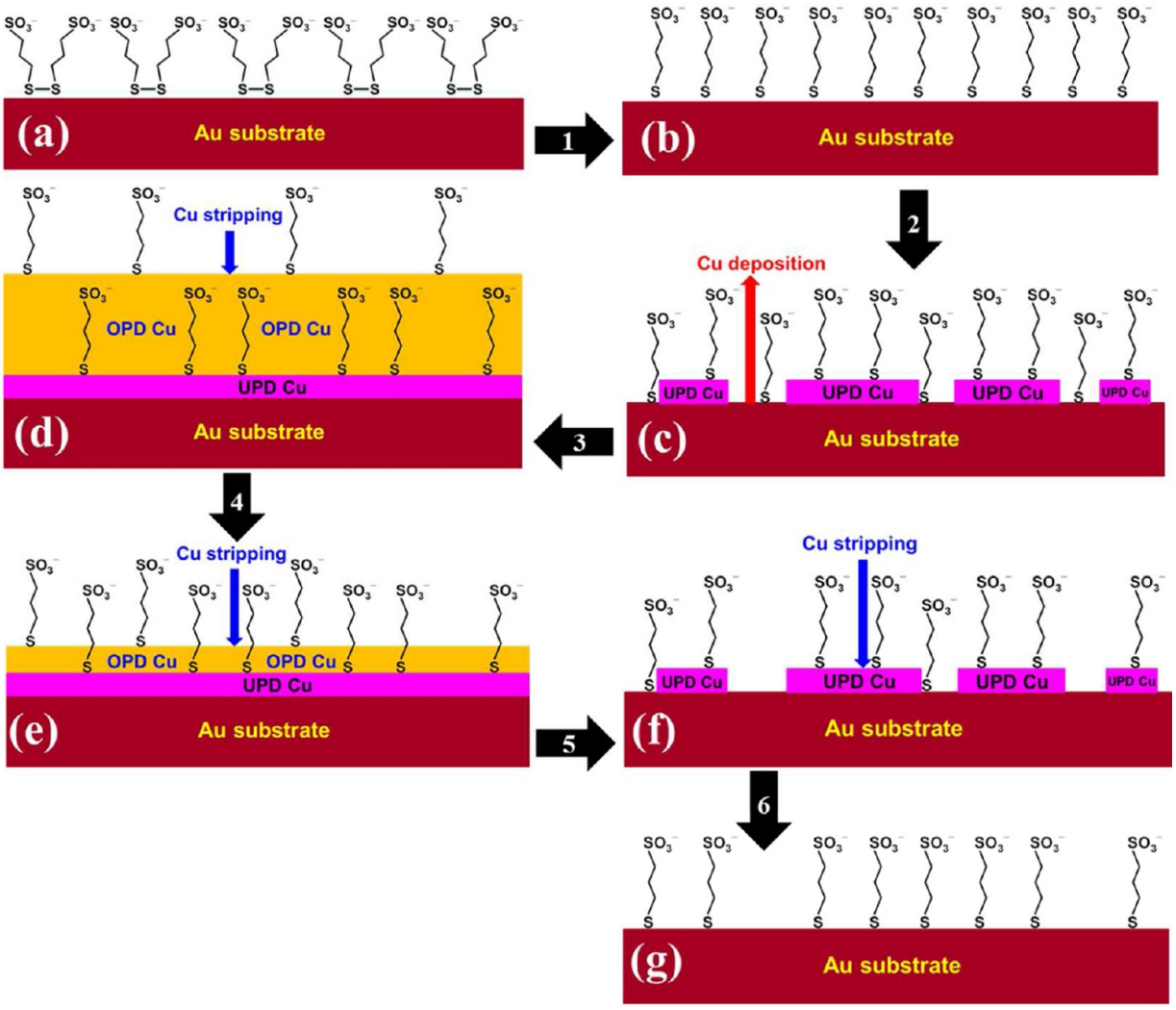

Figure 10. Schemes of SPS adsorption and desorption during Cu deposition and Cu dissolution at Au electrodes. (a) SPS-modified Au electrode. (b) Dissociation of SPS to MPS producing Au(I)-thiolates. (c) Cu UPD. Thiolates transfer from the Au surface to the top of Cu UPD layer. (d) Cu OPD. Most thiolates become buried by the Cu OPD layer. Some thiolates transfer to the top of the growing Cu film. (e) Cu OPD layer dissolution. Most thiolates desorb. (f) After Cu OPD layer dissolution. Buried thiolates are exposed to the solution. (g) After Cu UPD layer dissolution. Most thiolates readsorb on the Au electrode.

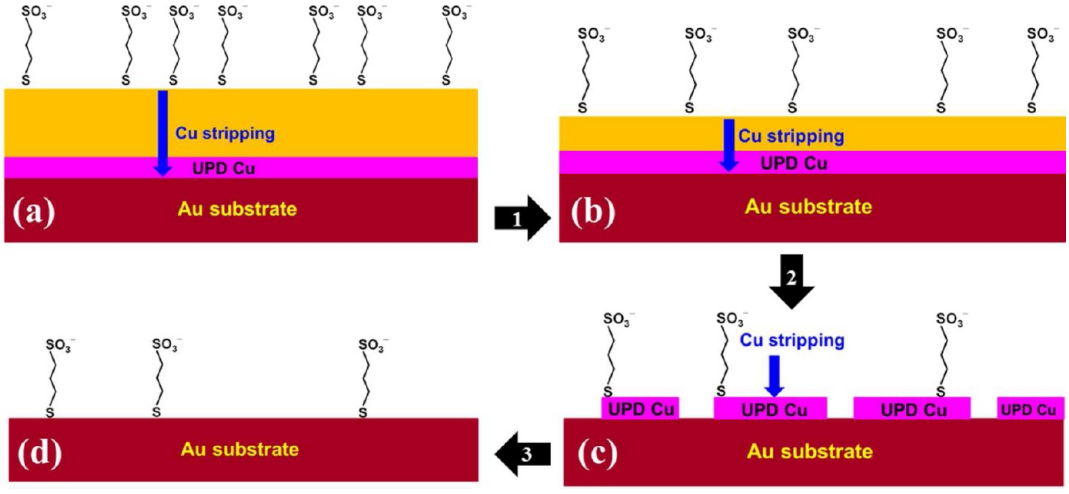

Figure 11. Schemes of SPS adsorption and desorption during Cu dissolution at Cu/Au electrodes. (a) SPS-modified Cu/Au electrode. Adsorbed SPS dissociates to MPS producing Cu(I)-thiolates. (b) Cu OPD layer dissolution. Most thiolates desorb. (c) After Cu OPD layer dissolution. Only a few thiolates readsorb on the Cu UPD layer. (d) After Cu UPD layer dissolution. Only a few thiolates readsorb on the Au electrode.

dx.doi.org/10.1021/la3025183 | *Langmuir* 2012, 28, 14476−14487

S(2p) signal intensity of the S−Au bond of sample B also decreases significantly toward lower TOAs. The decrease of the $C-SO_3^-$ signal with lowering the TOA is much smaller than the decrease of the S−Au signal with lowering the TOA, suggesting that the S−Au bond is located closer to the Au surface than the $C-SO_3^-$ bond. This is in agreement with the typical adsorption behavior of thiol molecules on Au electrodes (i.e., the thiol groups attach to the Au surface, whereas the SO_3^- groups point away from it).[49,51,52,54,87,88] Larger signal intensities at low TOAs for sample A suggest a much higher SPS coverage as compared to sample B, which is in agreement with the results of Figures 2 and 5.

3.5. Schemes for Cu Deposition and Cu Dissolution at SPS-modified Electrodes. On the basis of our experimental results, we propose two schemes to explain the adsorption and desorption processes of SPS during Cu growth and Cu dissolution at Au and Cu/Au electrodes.

3.5.1. Cu Growth and Dissolution at SPS-modified Au Electrodes. Figure 10 illustrates the adsorption and desorption processes of SPS during Cu deposition and dissolution at SPS-modified Au electrodes. First, SPS molecules adsorb on the Au surface and dissociate to thiolates (Figures 10, panels a and b) according to reaction 7.[26,53,58] A negative potential sweep initiates Cu growth. Cu atoms penetrate the thiolate adlayer and form the Cu UPD layer (Figure 10c). At more negative potentials, a uniform Cu OPD film is deposited. Thiolates which are strongly bonded to the Cu UPD layer are buried by the Cu OPD layer, whereas a part of the thiolates transfers to the perimeter of the Cu deposit (Figure 10d). In the reverse anodic potential sweep (i.e., during dissolution of the Cu film), the thiolates adsorbed on top of the Cu OPD layer either desorb into the solution bulk or return to the surface of the Cu UPD layer (Figures 10, panels e and f). Buried thiolates are exposed again to the electrolyte. After the stripping of the Cu UPD layer, the thiolates readsorb on the bare Au surface (Figure 10g).

3.5.2. Cu Dissolution at SPS-modified Cu/Au Electrodes. Figure 11 illustrates the adsorption and desorption processes of SPS during Cu dissolution at SPS-modified Cu/Au electrodes. In contrast to Figure 10, the SPS molecules are adsorbed on top of a precoated Cu film (Figure 11a). During dissolution of the Cu deposit at more positive potentials, most of the thiolates desorb into the solution bulk (Figure 11b). Only a small part of the thiolates readsorbs on the Cu UPD layer (Figure 11c) and on the bare Au surface (Figure 11d), respectively.

4. CONCLUSIONS

SPS dissociates to MPS upon adsorption on Au and Cu/Au electrodes to form Au(I)-thiolates and Cu(I)-thiolates. During Cu growth on the SPS-modified Au electrode, thiolates transfer from the Au surface to the top of the Cu UPD layer. The Cu UPD layer stabilizes the transferred thiolates against electrochemical reductive desorption. Therefore, most thiolates adsorbed on the Cu UPD layer are buried by the subsequent Cu OPD layer. A small part of thiolates transfers from the Cu UPD layer to the top of the growing Cu OPD layer because the relocation (i.e., readsorption) of the thiolates is kinetics controlled. The amount of the transferring thiolate is sufficient to accelerate Cu growth. When SPS molecules are preadsorbed on a Cu-coated Au electrode rather than a bare Au electrode most thiolates desorb into the bulk solution, and only a small part readsorbs onto the Au electrode after Cu is electrochemically stripped off. This work demonstrates that the amount of the SPS molecule needed to accelerate copper deposition is as low as a submonolayer. SPS molecules in the solution are not required. This information is important for the development of future plating bath formulations which allow Cu superfilling in modern electronic circuits.

■ ASSOCIATED CONTENT

Supporting Information

Assignments of XPS spectra in the S(2p) region. Charge value comparison of α peaks obtained from Figures 1, 2C, and 4. Potential ranges of Cu UPD in Figures 2 and 4. The best Cu-stripping peak fitting based on the sum of profiles δ and γ in Figure 6. Enlargement and comparison of Figure 4A. This material is available free of charge via the Internet at http://pubs.acs.org.

■ AUTHOR INFORMATION

Corresponding Author

*W.-P.D.: e-mail, dowwp@dragon.nchu.edu.tw; tel, 886-4-22859152; fax, 886-4-22854734. Y.-L.L.: e-mail, yllee@mail.ncku.edu.tw. S.-L.Y.: e-mail, yau6017@ncu.edu.tw.

Notes

The authors declare no competing financial interest.

■ ACKNOWLEDGMENTS

This work was supported by the National Science Council of Taiwan under Contract NSC 99-2221-E-005-096.

■ REFERENCES

(1) Ulman, A. *Chem. Rev.* **1996**, *96*, 1533.
(2) Christopher Love, J.; Estroff, L. A.; Kriebel, J. K.; Nuzzo, R. G.; Whitesides, G. M. *Chem. Rev.* **2005**, *105*, 1103.
(3) Herzog, G.; Arrigan, D. W. M. *Anal. Chem.* **2003**, *75*, 319.
(4) Schlenoff, J. B.; Li, M.; Ly, H. *J. Am. Chem. Soc.* **1995**, *117*, 12528.
(5) Poirier, G. E. *Chem. Rev.* **1997**, *97*, 1117.
(6) Schreiber, F. *Prog. Surf. Sci.* **2000**, *65*, 151.
(7) Kudelski, A.; Pecul, M.; Bukowska, J. *J. Raman Spectrosc.* **2002**, *33*, 796.
(8) Kudelski, A. *Langmuir* **2002**, *18*, 4741.
(9) Kudelski, A. *Langmuir* **2003**, *19*, 3805.
(10) Mokrani, C.; Fatisson, J.; Guérente, L.; Labbé, P. *Langmuir* **2005**, *21*, 4400.
(11) Ooi, Y.; Hobara, D.; Yamamoto, M.; Kakiuchi, T. *Langmuir* **2005**, *21*, 11185.
(12) Baunach, T.; Ivanova, V.; Kolb, D. M.; Boyen, H.-G.; Ziemann, P.; Büttner, M.; Oelhafen, P. *Adv. Mater. (Weinheim, Ger.)* **2004**, *16*, 2024.
(13) Madueno, R.; Räisänen, M. T.; Silien, C.; Buck, M. *Nature* **2008**, *454*, 618.
(14) Silien, C.; Räisänen, M. T.; Buck, M. *Angew. Chem., Int. Ed.* **2009**, *48*, 3349.
(15) Schneeweiss, M. A.; Hagenström, H.; Esplandiu, M. J.; Kolb, D. M. *Appl. Phys. A: Mater. Sci. Process.* **1999**, *69*, 537.
(16) Esplandiu, M. J.; Hagenström, H. *Solid State Ionics* **2002**, *150*, 39.
(17) Nishizawa, M.; Sunagawa, T.; Yoneyama, H. *Langmuir* **1997**, *13*, 5215.
(18) Oyamatsu, D.; Nishizawa, M.; Kuwabata, S.; Yoneyama, H. *Langmuir* **1998**, *14*, 3298.
(19) Cavalleri, O.; Kind, H.; Bittner, A. M.; Kern, K. *Langmuir* **1998**, *14*, 7292.
(20) Oyamatsu, D.; Kuwabata, S.; Yoneyama, H. *J. Electroanal. Chem.* **1999**, *473*, 59.
(21) Hagenström, H.; Schneeweiss, M. A.; Kolb, D. M. *Langmuir* **1999**, *15*, 7802.

(22) Hagenström, H.; Schneeweiss, M. A.; Kolb, D. M. *Electrochim. Acta* **1999**, *45*, 1141.
(23) Hagenström, H.; Esplandiú, M. J.; Kolb, D. M. *Langmuir* **2001**, *17*, 839.
(24) Petri, M.; Kolb, D. M.; Memmert, U.; Meyer, H. *Electrochim. Acta* **2003**, *49*, 183.
(25) Silien, C.; Buck, M. *J. Phys. Chem. C* **2008**, *112*, 3881.
(26) Yanson, Y.; Frenken, J. W. M.; Rost, M. J. *Phys. Chem. Chem. Phys.* **2011**, *13*, 16095.
(27) Cavalleri, O.; Gilbert, S. E.; Kern, K. *Chem. Phys. Lett.* **1997**, *269*, 479.
(28) Cavalleri, O.; Gilbert, S. E.; Kern, K. *Surf. Sci.* **1997**, *377*−*379*, 931.
(29) Moffat, T. P.; Wheeler, D.; Josell, D. *J. Electrochem. Soc.* **2004**, *151*, C262.
(30) Dow, W.-P.; Chiu, Y.-D.; Yen, M.-Y. *J. Electrochem. Soc.* **2009**, *156*, D155.
(31) Moffat, T. P.; Wheeler, D.; Huber, W. H.; Josell, D. *Electrochem. Solid-State Lett.* **2001**, *4*, C26.
(32) West, A. C.; Mayer, S.; Reid, J. *Electrochem. Solid-State Lett.* **2001**, *4*, C50.
(33) Moffat, T. P.; Wheeler, D.; Witt, C.; Josell, D. *Electrochem. Solid-State Lett.* **2002**, *5*, C110.
(34) Dow, W.-P.; Yen, M.-Y. *Electrochem. Solid-State Lett.* **2005**, *8*, C161.
(35) Dow, W.-P.; Li, C.-C.; Lin, M.-W.; Su, G.-W.; Huang, C.-C. *J. Electrochem. Soc.* **2009**, *156*, D314.
(36) Carvalhal, R. F.; Freire, R. S.; Kubota, L. T. *Electroanalysis* **2005**, *17*, 1251.
(37) Tkac, J.; Davis, J. J. *J. Electroanal. Chem.* **2008**, *621*, 117.
(38) Chiu, Y.-D.; Dow, W.-P.; Huang, S.-M.; Yau, S.-L.; Lee, Y.-L. *J. Electrochem. Soc.* **2011**, *158*, D290.
(39) Vereecken, P. M.; Binstead, R. A.; Deligianni, H.; Andricacos, P. C. *IBM J. Res. Dev.* **2005**, *49*, 3.
(40) Krug, K.; Liu, Y.-F.; Ho, W.-H.; Lee, Y.-L.; Dow, W.-P.; Yau, S.-L. *J. Phys. Chem. C* **2012**, *116*, 17507.
(41) Yang, D.-F.; Al-Maznai, H.; Morin, M. *J. Phys. Chem. B* **1997**, *101*, 1158.
(42) Loglio, F.; Schweizer, M.; Kolb, D. M. *Langmuir* **2003**, *19*, 830.
(43) Campiña, J. M.; Martins, A.; Silva, F. *Electrochim. Acta* **2008**, *53*, 7681.
(44) Yokoi, M.; Konishi, S.; Hayashi, T. *Denki Kagaku oyobi Kogyo Butsuri Kagaku* **1984**, *52*, 218.
(45) Reid, J. D.; David, A. P. *Plat. Surf. Finish.* **1987**, *74*, 66.
(46) Healy, J. P.; Pletcher, D.; Goodenough, M. *J. Electroanal. Chem.* **1992**, *338*, 155.
(47) Feng, Z. V.; Li, X.; Gewirth, A. A. *J. Phys. Chem. B* **2003**, *107*, 9415.
(48) Dow, W.-P.; Yen, M.-Y.; Lin, W.-B.; Ho, S.-W. *J. Electrochem. Soc.* **2005**, *152*, C769.
(49) Moffat, T. P.; Ou Yang, L.-Y. *J. Electrochem. Soc.* **2010**, *157*, D228.
(50) Garcia-Cardona, E.; Wong, E. H.; Barkey, D. P. *J. Electrochem. Soc.* **2011**, *158*, D143.
(51) Broekmann, P.; Fluegel, A.; Emnet, C.; Arnold, M.; Roeger-Goepfert, C.; Wagner, A.; Hai, N. T. M.; Mayer, D. *Electrochim. Acta* **2011**, *56*, 4724.
(52) Hai, N. T. M.; Huynh, T. T. M.; Fluegel, A.; Arnold, M.; Mayer, D.; Reckien, W.; Bredow, T.; Broekmann, P. *Electrochim. Acta* **2012**, *70*, 286.
(53) Liu, Y.-F.; Lee, Y.-L.; Yang, Y.-C.; Jian, Z.-Y.; Dow, W.-P.; Yau, S.-L. *Langmuir* **2010**, *26*, 13263.
(54) Tu, H. L.; Yen, P. Y.; Chen, S.; Yau, S.-L.; Dow, W.-P.; Lee, Y.-L. *Langmuir* **2011**, *27*, 6801.
(55) Jennings, G. K.; Laibinis, P. E. *Langmuir* **1996**, *12*, 6173.
(56) Jennings, G. K.; Laibinis, P. E. *J. Am. Chem. Soc.* **1997**, *119*, 5208.
(57) Zamborini, F. P.; Campbell, J. K.; Crooks, R. M. *Langmuir* **1998**, *14*, 640.
(58) Jian, Z.-Y.; Chang, T.-Y.; Yang, Y.-C.; Dow, W.-P.; Yau, S.-L.; Lee, Y.-L. *Langmuir* **2009**, *25*, 179.
(59) Benedetti, A. V.; Sumodjo, P. T. A.; Nobe, K.; Cabot, P. L.; Proud, W. G. *Electrochim. Acta* **1995**, *40*, 2657.
(60) Ma, H. Y.; Yang, C.; Yin, B. S.; Li, G. Y.; Chen, S. H.; Luo, J. L. *Appl. Surf. Sci.* **2003**, *218*, 143.
(61) Láng, G. G.; Ujvári, M.; Horányi, G. *J. Electroanal. Chem.* **2002**, *522*, 179.
(62) Doblhofer, K.; Wasle, S.; Soares, D. M.; Weil, K. G.; Ertl, G. *J. Electrochem. Soc.* **2003**, *150*, C657.
(63) Okubo, T.; Watanabe, K.; Kondo, K. *J. Electrochem. Soc.* **2007**, *154*, C181.
(64) Dow, W.-P.; Huang, H.-S.; Lin, Z. *Electrochem. Solid-State Lett.* **2003**, *6*, C134.
(65) Nagy, Z.; Blaudeau, J. P.; Hung, N. C.; Curtiss, L. A.; Zurawski, D. J. *J. Electrochem. Soc.* **1995**, *142*, L87.
(66) Bard, A. J.; Faulkner, L. R. *Electrochemical Methods: Fundamentals and Applications*, 2nd ed.; John Wiley & Sons, Inc.: New York, 2001; pp 115−116.
(67) Lee, H. P.; Nobe, K. *J. Electrochem. Soc.* **1986**, *133*, 2035.
(68) Crundwell, F. K. *Electrochim. Acta* **1992**, *37*, 2707.
(69) Soares, D. M.; Wasle, S.; Weil, K. G.; Doblhofer, K. *J. Electroanal. Chem.* **2002**, *532*, 353.
(70) Dow, W.-P.; Huang, H.-S.; Yen, M.-Y.; Chen, H.-H. *J. Electrochem. Soc.* **2005**, *152*, C77.
(71) Evans, S. D.; Ulman, A.; Goppert-Berarducci, K. E.; Gerenser, L. J. *J. Am. Chem. Soc.* **1991**, *113*, 5866.
(72) Tarlov, M. J.; Burgess, D. R. F., Jr.; Gillen, G. *J. Am. Chem. Soc.* **1993**, *115*, 5305.
(73) Laibinis, P. E.; Whitesides, G. M.; Allara, D. L.; Tao, Y.-T.; Parikh, A. N.; Nuzzo, R. G. *J. Am. Chem. Soc.* **1991**, *113*, 7152.
(74) Freeman, T. L.; Evans, S. D.; Ulman, A. *Langmuir* **1995**, *11*, 4411.
(75) Castner, D. G.; Hinds, K.; Grainger, D. W. *Langmuir* **1996**, *12*, 5083.
(76) Lee, M.-T.; Hsueh, C.-C.; Freund, M. S.; Ferguson, G. S. *Langmuir* **1998**, *14*, 6419.
(77) Hutt, D. A.; Leggett, G. J. *J. Phys. Chem.* **1996**, *100*, 6657.
(78) Rieley, H.; Kendall, G. K.; Zemicael, F. W.; Smith, T. L.; Yang, S. *Langmuir* **1998**, *14*, 5147.
(79) Wang, X.; Lieberman, M. *Langmuir* **2003**, *19*, 7346.
(80) Ang, T. P.; Wee, T. S. A.; Chin, W. S. *J. Phys. Chem. B* **2004**, *108*, 11001.
(81) Zhang, H.-L.; Evans, S. D.; Critchley, K.; Fukushima, H.; Tamaki, T.; Fournier, F.; Zheng, W.; Carrez, S.; Dubost, H.; Bourguignon, B. *J. Chem. Phys.* **2005**, *122*, 224707.
(82) Pranger, L.; Goldstein, A.; Tannenbaum, R. *Langmuir* **2005**, *21*, 5396.
(83) Amato, C.; Devillers, S.; Calas, P.; Delhalle, J.; Mekhalif, Z. *Langmuir* **2008**, *24*, 10879.
(84) Caprioli, F.; Beccari, M.; Martinelli, A.; Castro, V. D.; Decker, F. *Phys. Chem. Chem. Phys.* **2009**, *11*, 11624.
(85) García-Raya, D.; Madueño, R.; Blázquez, M.; Pineda, T. *J. Phys. Chem. C* **2010**, *114*, 3568.
(86) Feng, Y.; Teo, W.-K.; Siow, K.-S.; Gao, Z.; Tan, K.-L.; Hsieh, A.-K. *J. Electrochem. Soc.* **1997**, *144*, 55.
(87) Bain, C. D.; Troughton, E. B.; Tao, Y.-T.; Evall, J.; Whitesides, G. M.; Nuzzo, R. G. *J. Am. Chem. Soc.* **1989**, *111*, 321.
(88) Wirde, M.; Gelius, U.; Nyholm, L. *Langmuir* **1999**, *15*, 6370.

Supporting Information

Adsorption and Desorption of Bis-(3-sulfopropyl) Disulfide during Cu Electrodeposition and Stripping at Au Electrodes

Yong-Da Chiu,[†] Wei-Ping Dow,[†,*]

Klaus Krug,[§] Yung-Fang Liu,[§] Yuh-Lang Lee,[§,*]

Shueh-Lin Yau,[‡,*]

[†] Department of Chemical Engineering, National Chung Hsing University, Taichung 40227, Taiwan

[§] Department of Chemical Engineering, National Cheng Kung University, Tainan 70101, Taiwan

[‡] Department of Chemistry, National Central University, Jhong-Li, Tao-Yuan 32001, Taiwan

*** Corresponding author.** E-mail: dowwp@dragon.nchu.edu.tw (W.-P. Dow); yllee@mail.ncku.edu.tw (Y.-L Lee); yau6017@ncu.edu.tw (S.-L Yau); Tel: 886-4-22859152 (W.-P. Dow); Fax: 886-4-22854734 (W.-P. Dow).

Table S1. Assignments of XPS spectra in the S(2p) region

Binding energy (eV)	Assignment (species)	References
161.8($2p_{3/2}$), 162($2p_{3/2}$), 163.2($2p_{1/2}$),	R-S-Au	71, 72, 76, 77, 79, 81, 85
162/163, 161.9, 162.6($2p_{3/2}$),		73, 78, 79, 81
163.1($2p_{1/2}$), 163.9($2p_{1/2}$)		81, 85
161.9($2p_{3/2}$)	R-S-Au[a]	75
163.1($2p_{3/2}$)	R-S-Au[b]	75
162.1($2p_{3/2}$), 163.3($2p_{1/2}$), 162.4($2p_{3/2}$),	R-S-Cu	73, 74, 80, 86
163.6($2p_{1/2}$), 162.7($2p_{3/2}$), 163.9($2p_{1/2}$)		80, 82, 86
162.6($2p_{3/2}$), 162.3, 162.4, 162.5		83, 84
163.5, 163.6-164.8,	R-S-Cu^{2+}	71, 74
163.6-164.8, 163.5($2p_{3/2}$),165($2p_{1/2}$)	R-SH	74, 75, 85
163.8($2p_{3/2}$), 163.4		83, 84
163.5-164($2p_{3/2}$), 164, 165.2, 164.8	R-S-S-R’	75, 79
167, 167.4($2p_{3/2}$), 169, 168($2p_{3/2}$)	R-SO_3^-	65, 73, 76, 77, 78, 82, 83
169.4($2p_{1/2}$), 168, 168.2		82, 86
168($2p_{3/2}$), 169.2($2p_{1/2}$), 165.5($2p_{3/2}$)	R-SO_2-R’	74, 83
162($2p_{3/2}$), 163.2($2p_{1/2}$)	R-S-Au	this work
168($2p_{3/2}$), 169($2p_{1/2}$)	Au-R-SO_3^-	this work
162($2p_{3/2}$), 163.6($2p_{1/2}$)	R-S-Cu	this work
168($2p_{3/2}$), 169($2p_{1/2}$)	Cu-R-SO_3^-	this work

[a] thiolates bound to threefold hollow sites.
[b] thiolates bound to lower coordination sites.

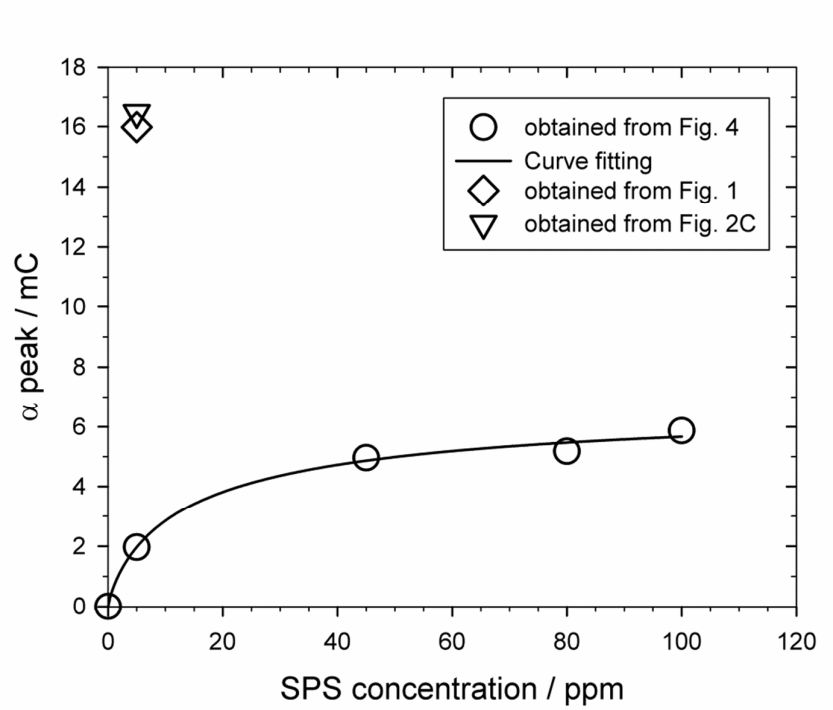

Figure S1. Charge value comparison of α peaks. The raw data are obtained from Figs. 1 and 2C and 4. The relationship between the SPS concentration (i.e., the surface coverage of thiolate) and the charge amount of the α peak obtained from Fig. 4 fits a Langmuir-like adsorption isotherm, which is in agreement with our previous work (i.e., *J. Electrochem. Soc.* **2011**, *158*, D290).

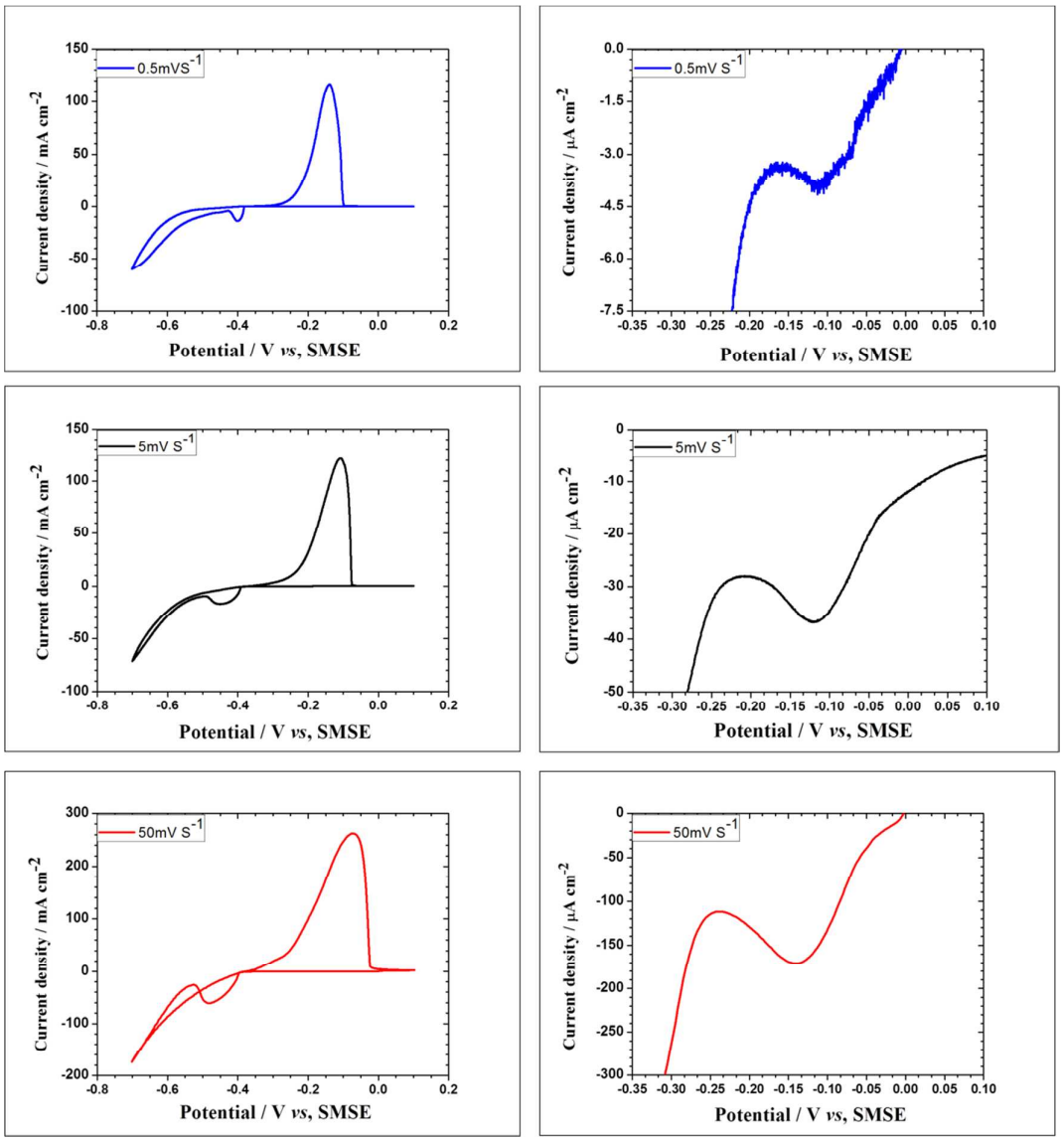

Figure S2. Potential ranges of Cu UPD in Fig. 2. The left-side Figures are the original CV patterns shown in Fig. 2. The right-side Figures are the corresponding enlargements to show the potential ranges of Cu UPD. The Cu UPD peaks are explained in our previous work (i.e., *Int. J. Electrochem. Soc.* **2011**, *6*, 3416).

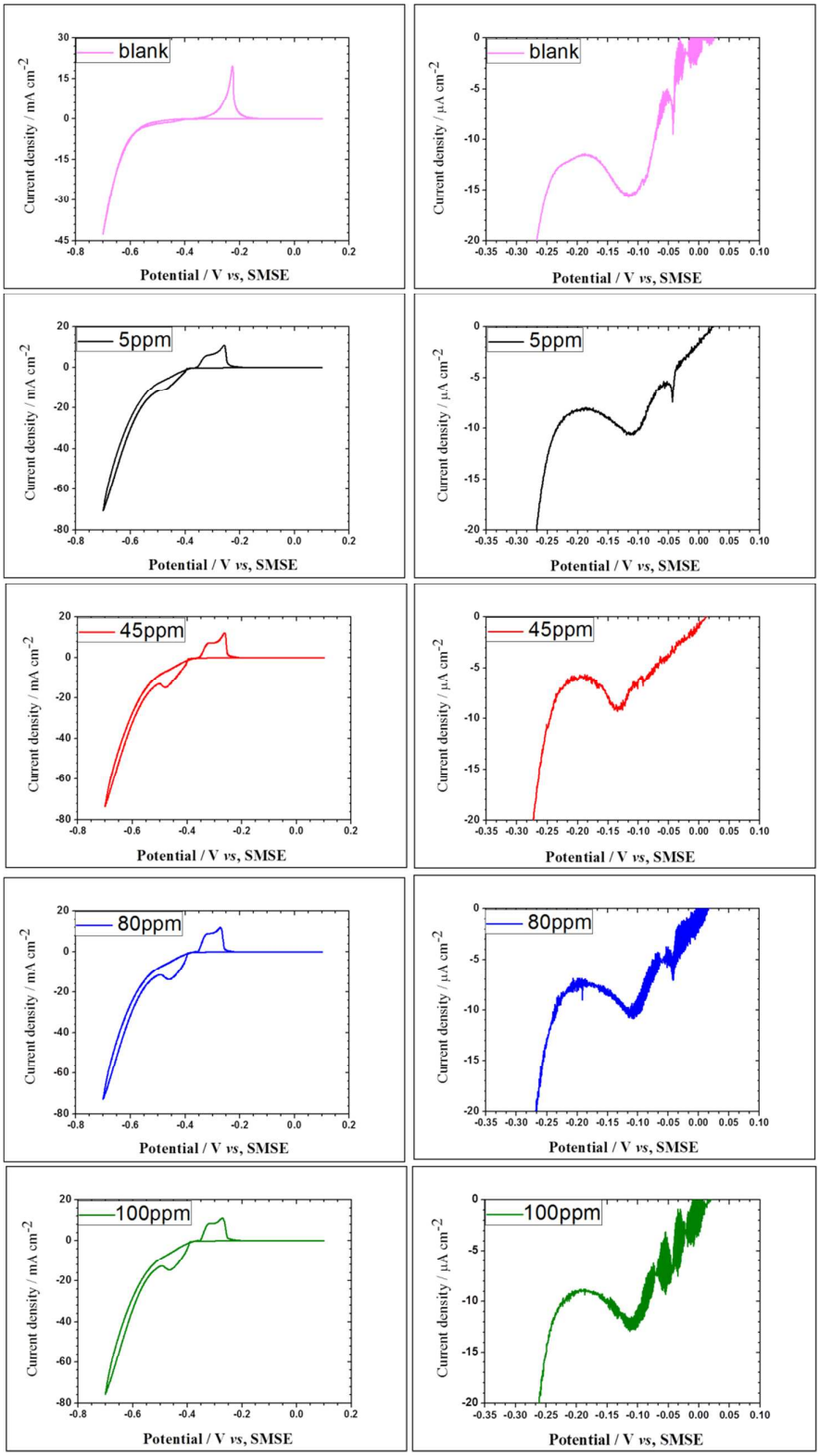

Figure S3. Potential ranges of Cu UPD in Fig. 4. The left-side Figures are the original CV patterns shown in Fig. 4. The right-side Figures are the corresponding enlargements to show the potential ranges of Cu UPD. One shape and one broad Cu UPD peaks are explained in a previous work (i.e., *Int. J. Electrochem. Soc.* **2011**, *6*, 3416).

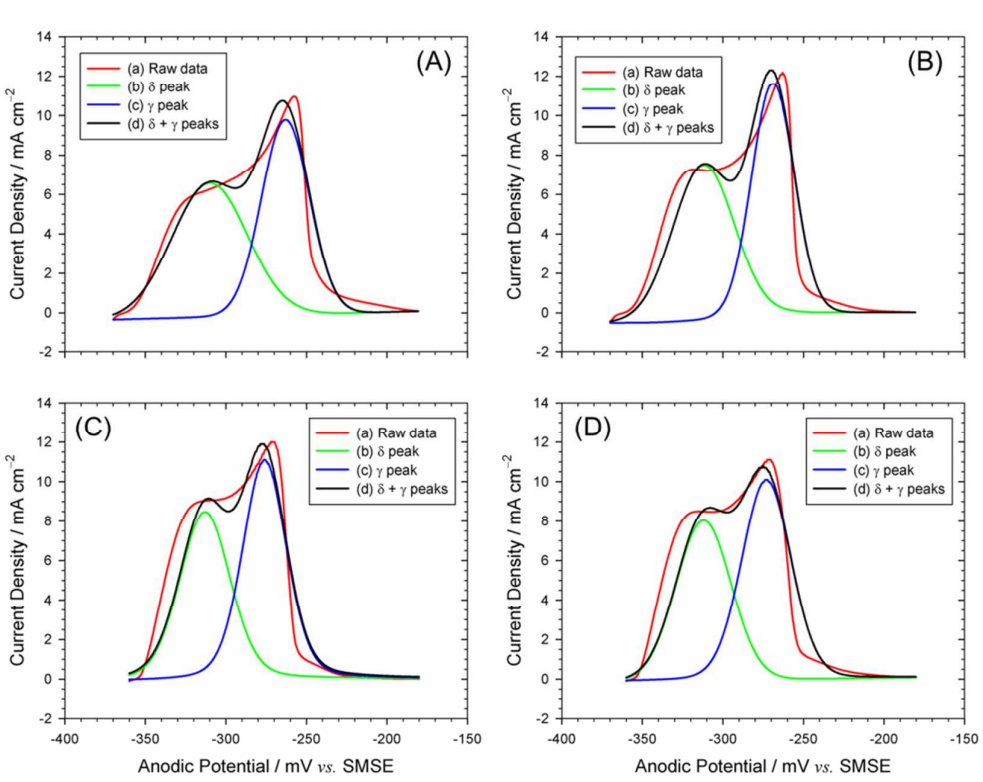

Figure S4. Cu stripping peaks for SPS-modified Cu/Au electrodes in 0.54M H_2SO_4 containing 0.88M $CuSO_4$, 200ppm PEG, and 70ppm Cl^- (curves a) and corresponding best fits (curves d) based on the sum of two profiles δ (curves b) and γ (curves c). The SPS concentrations in the pre-adsorption baths were (A) 5 ppm, (B) 45 ppm, (C) 80 ppm, (D) 100 ppm.

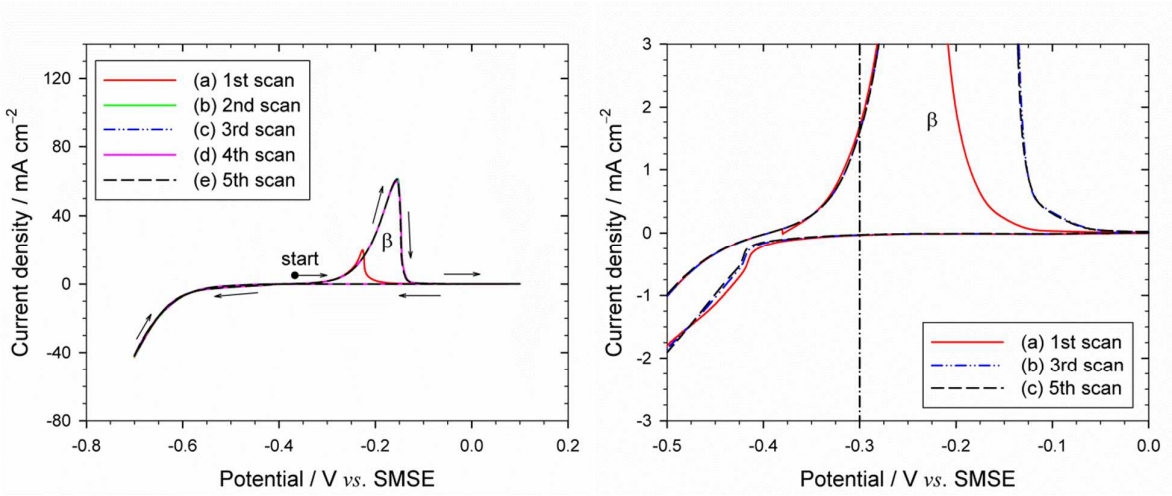

Figure S5. Enlargement and comparison of Fig. 4A. The current density of copper stripping at −0.3 V is about 1.5 mA cm^{-2} in the absence of SPS. In contrast with Fig. S4, these current densities of copper stripping at −0.3 V always are higher than 7 mA cm^{-2} due to the SPS pre-adsorption on the copper surfaces.